Fano resonances in the nonlinear optical response of coupled plasmonic nanostructures

Jérémy Butet* and Olivier J. F. Martin

Nanophotonics and Metrology Laboratory (NAM), Swiss Federal Institute of Technology Lausanne (EPFL), 1015, Lausanne, Switzerland
**jeremy.butet@epfl.ch*

Abstract: The coupling between metallic nanostructures is a common and easy way to control the optical properties of plasmonic systems. Even though the coupling between plasmonic oscillators has been widely studied in the linear regime, its influence on the nonlinear optical response of metallic nanostructures has been sparsely considered. Using a surface integral equation method, we investigate the second order nonlinear optical response of plasmonic metamolecules supporting Fano resonances revealing that the typical lineshape of Fano resonances is also clearly observable in the nonlinear regime. The physical mechanisms leading to nonlinear Fano resonances are revealed by the coupled oscillator model and the symmetry subgroup decomposition. It is found that the origin of the nonlinear scattered wave, i. e. the active plasmonic oscillator, can be selectively chosen. Furthermore, interferences between nonlinear emissions are clearly observed in specific configurations. The results presented in this article pave the way for the design of efficient nonlinear plasmonic metamolecules with controlled nonlinear radiation.

OCIS codes: (160.3900) Metals; (190.0190) Nonlinear optics; (190.2620) Harmonic generation and mixing; (280.4788) Optical sensing and sensors; (160.4236) Nanomaterials.

References and links

1. U. Fano, "Sullo spettro di assorbimento dei gas nobili presso il limite dello spettro d'arco," Nuovo Cim. **12**(3), 154–161 (1935).
2. U. Fano, "Effects of configuration interaction on intensities and phase shifts," Phys. Rev. **124**(6), 1866–1878 (1961).
3. M. V. Rybin, A. B. Khanikaev, M. Inoue, K. B. Samusev, M. J. Steel, G. Yushin, and M. F. Limonov, "Fano resonance between Mie and Bragg scattering in photonic crystals," Phys. Rev. Lett. **103**(2), 023901 (2009).
4. A. R. P. Rau, "Perspectives on the Fano resonance formula," Phys. Scr. **69**(1), C10–C13 (2004).
5. A. E. Miroshnichenko, S. Flach, and Y. S. Kivshar, "Fano resonances in nanoscale structures," Rev. Mod. Phys. **82**(3), 2257–2298 (2010).
6. B. Luk'yanchuk, N. I. Zheludev, S. A. Maier, N. J. Halas, P. Nordlander, H. Giessen, and C. T. Chong, "The Fano resonance in plasmonic nanostructures and metamaterials," Nat. Mater. **9**(9), 707–715 (2010).
7. M. Rahmani, B. Luk'yanchuck, and M. Hong, "Fano resonance in novel plasmonic nanostructures," Laser Phot. Rev. **7**(3), 329–349 (2013).
8. S. Zhang, D. A. Genov, Y. Wang, M. Liu, and X. Zhang, "Plasmon-induced transparency in metamaterials," Phys. Rev. Lett. **101**(4), 047401 (2008).
9. F. Hao, P. Nordlander, Y. Sonnefraud, P. Van Dorpe, and S. A. Maier, "Tunability of subradiant dipolar and Fano-type plasmon resonances in metallic ring/disk cavities: implications for nanoscale optical sensing," ACS Nano **3**(3), 643–652 (2009).
10. N. Verellen, Y. Sonnefraud, H. Sobhani, F. Hao, V. V. Moshchalkov, P. Van Dorpe, P. Nordlander, and S. A. Maier, "Fano resonances in individual coherent plasmonic nanocavities," Nano Lett. **9**(4), 1663–1667 (2009).
11. N. Liu, T. Weiss, M. Mesch, L. Langguth, U. Eigenthaler, M. Hirscher, C. Sönnichsen, and H. Giessen, "Planar metamaterial analogue of electromagnetically induced transparency for plasmonic sensing," Nano Lett. **10**(4), 1103–1107 (2010).
12. J. B. Lassiter, H. Sobhani, J. A. Fan, J. Kundu, F. Capasso, P. Nordlander, and N. J. Halas, "Fano resonances in plasmonic nanoclusters: geometrical and chemical tunability," Nano Lett. **10**(8), 3184–3189 (2010).
13. J. A. Fan, C. Wu, K. Bao, J. Bao, R. Bardhan, N. J. Halas, V. N. Manoharan, P. Nordlander, G. Shvets, and F. Capasso, "Self-assembled plasmonic nanoparticle clusters," Science **328**(5982), 1135–1138 (2010).
14. M. Hentschel, M. Saliba, R. Vogelgesang, H. Giessen, A. P. Alivisatos, and N. Liu, "Transition from isolated to collective modes in plasmonic oligomers," Nano Lett. **10**(7), 2721–2726 (2010).

#224277 - $15.00 USD Received 2 Oct 2014; revised 10 Nov 2014; accepted 10 Nov 2014; published 20 Nov 2014

15. M. Hentschel, D. Dregely, R. Vogelgesang, H. Giessen, and N. Liu, "Plasmonic oligomers: The role of individual particles in collective behavior," ACS Nano **5**(3), 2042–2050 (2011).
16. Y. H. Fu, J. B. Zhang, Y. F. Yu, and B. Luk'yanchuk, "Generating and manipulating higher order Fano resonances in dual-disk ring plasmonic nanostructures," ACS Nano **6**(6), 5130–5137 (2012).
17. A. E. Cetin and H. Altug, "Fano resonant ring/disk plasmonic nanocavities on conducting substrates for advanced biosensing," ACS Nano **6**(11), 9989–9995 (2012).
18. C. Wu, A. B. Khanikaev, R. Adato, N. Arju, A. A. Yanik, H. Altug, and G. Shvets, "Fano-resonant asymmetric metamaterials for ultrasensitive spectroscopy and identification of molecular monolayers," Nat. Mater. **11**(1), 69–75 (2011).
19. J. Ye, F. Wen, H. Sobhani, J. B. Lassiter, P. Van Dorpe, P. Nordlander, and N. J. Halas, "Plasmonic nanoclusters: Near-Field properties of the Fano resonance interrogated with Sers," Nano Lett. **12**(3), 1660–1667 (2012).
20. B. Gallinet and O. J. F. Martin, "Ab-initio theory of Fano resonances in plasmonic nanostructures and metamaterials," Phys. Rev. B **83**(23), 235427 (2011).
21. B. Gallinet and O. J. F. Martin, "Influence of electromagnetic interactions on the line shape of plasmonic Fano resonances," ACS Nano **5**(11), 8999–9008 (2011).
22. V. Giannini, Y. Francescato, H. Amrania, C. C. Phillips, and S. A. Maier, "Fano resonances in nanoscale plasmonic systems: A parameter-free modeling approach," Nano Lett. **11**(7), 2835–2840 (2011).
23. B. Gallinet and O. J. F. Martin, "Relation between near-field and far-field properties of plasmonic Fano resonances," Opt. Express **19**(22), 22167–22175 (2011).
24. N. Verellen, P. Van Dorpe, C. Huang, K. Lodewijks, G. A. E. Vandenbosch, L. Lagae, and V. V. Moshchalkov, "Plasmon line shaping using nanocrosses for high sensitivity localized surface plasmon resonance sensing," Nano Lett. **11**(2), 391–397 (2011).
25. M. Rahmani, D. Y. Lei, V. Giannini, B. Lukiyanchuk, M. Ranjbar, T. Y. F. Liew, M. Hong, and S. A. Maier, "Subgroup decomposition of plasmonic resonances in hybrid oligomers: modeling the resonance lineshape," Nano Lett. **12**(4), 2101–2106 (2012).
26. A. Lovera, B. Gallinet, P. Nordlander, and O. J. F. Martin, "Mechanisms of Fano resonances in coupled plasmonic systems," ACS Nano **7**(5), 4527–4536 (2013).
27. M. Kauranen and A. V. Zayats, "Nonlinear plasmonics," Nat. Photonics **6**(11), 737–748 (2012).
28. J. Butet, J. Duboisset, G. Bachelier, I. Russier-Antoine, E. Benichou, C. Jonin, and P.-F. Brevet, "Optical second harmonic generation of single metallic nanoparticles embedded in a homogeneous medium," Nano Lett. **10**(5), 1717–1721 (2010).
29. J. Butet, G. Bachelier, I. Russier-Antoine, C. Jonin, E. Benichou, and P.-F. Brevet, "Interference between selected dipoles and octupoles in the optical second-harmonic generation from spherical gold nanoparticles," Phys. Rev. Lett. **105**(7), 077401 (2010).
30. Y. Zhang, N. K. Grady, C. Ayala-Orozco, and N. J. Halas, "Three-dimensional nanostructures as highly efficient generators of second harmonic light," Nano Lett. **11**(12), 5519–5523 (2011).
31. H. Husu, R. Siikanen, J. Mäkitalo, J. Lehtolahti, J. Laukkanen, M. Kuittinen, and M. Kauranen, "Metamaterials with tailored nonlinear optical response," Nano Lett. **12**(2), 673–677 (2012).
32. M. Castro-Lopez, D. Brinks, R. Sapienza, and N. F. van Hulst, "Aluminum for nonlinear plasmonics: Resonance-driven polarized luminescence of Al, Ag, and Au nanoantennas," Nano Lett. **11**(11), 4674–4678 (2011).
33. P. Biagioni, D. Brida, J.-S. Huang, J. Kern, L. Duò, B. Hecht, M. Finazzi, and G. Cerullo, "Dynamics of four-photon photoluminescence in gold nanoantennas," Nano Lett. **12**(6), 2941–2947 (2012).
34. K. D. Ko, A. Kumar, K. H. Fung, R. Ambekar, G. L. Liu, N. X. Fang, K. C. Toussaint, Jr., and C. Toussaint, "Nonlinear optical response from arrays of Au bowtie nanoantennas," Nano Lett. **11**(1), 61–65 (2011).
35. M. Lippitz, M. A. van Dijk, and M. Orrit, "Third-harmonic generation from single gold nanoparticles," Nano Lett. **5**(4), 799–802 (2005).
36. O. Schwartz and D. Oron, "Background-free third harmonic imaging of gold nanorods," Nano Lett. **9**(12), 4093–4097 (2009).
37. M. Hentschel, T. Utikal, H. Giessen, and M. Lippitz, "Quantitative modeling of the third harmonic emission spectrum of plasmonic nanoantennas," Nano Lett. **12**(7), 3778–3782 (2012).
38. M. Navarro-Cia and S. A. Maier, "Broad-band near-infrared plasmonic nanoantennas for higher harmonic generation," ACS Nano **6**(4), 3537–3544 (2012).
39. M. Danckwerts and L. Novotny, "Optical frequency mixing at coupled gold nanoparticles," Phys. Rev. Lett. **98**(2), 026104 (2007).
40. F. Hache, D. Ricard, C. Flytzanis, and U. Kreibig, "The optical Kerr effect in small metal particles and metal colloids: The case of gold," App. Phys. A **47**(4), 347–357 (1988).
41. K. Thyagarajan, J. Butet, and O. J. F. Martin, "Augmenting second harmonic generation using Fano resonances in plasmonic systems," Nano Lett. **13**(4), 1847–1851 (2013).
42. Y. Zhang, F. Wen, Y. R. Zhen, P. Nordlander, and N. J. Halas, "Coherent Fano resonances in a plasmonic nanocluster enhance optical four-wave mixing," Proc. Natl. Acad. Sci. U.S.A. **110**(23), 9215–9219 (2013).
43. G. F. Walsh and L. Dal Negro, "Enhanced second harmonic generation by photonic-plasmonic Fano-type coupling in nanoplasmonic arrays," Nano Lett. **13**(7), 3111–3117 (2013).
44. J. Butet and O. J. F. Martin, "Nonlinear plasmonic nanorulers," ACS Nano **8**(5), 4931–4939 (2014).
45. Y. Zhang, Y.-R. Zhen, O. Neumann, J. K. Day, P. Nordlander, and N. J. Halas, "Coherent anti-Stokes Raman scattering with single-molecule sensitivity using a plasmonic Fano resonance," Nat Commun **5**, 4424 (2014).

#224277 - $15.00 USD Received 2 Oct 2014; revised 10 Nov 2014; accepted 10 Nov 2014; published 20 Nov 2014

46. J. Butet, I. Russier-Antoine, C. Jonin, N. Lascoux, E. Benichou, and P.-F. Brevet, "Sensing with multipolar second harmonic generation from spherical metallic nanoparticles," Nano Lett. **12**(3), 1697–1701 (2012).
47. J. Butet and O. J. F. Martin, "Refractive index sensing with Fano resonant plasmonic nanostructures: A symmetry based nonlinear approach," Nanoscale, Accepted article (2014). DOI: 10.1039/C4NR05623J.
48. A. M. Kern and O. J. F. Martin, "Surface integral formulation for 3D simulation of plasmonic and high permittivity nanostructures," J. Opt. Soc. Am. A **26**(4), 732–740 (2009).
49. J. Mäkitalo, S. Suuriniemi, and M. Kauranen, "Boundary element method for surface nonlinear optics of nanoparticles," Opt. Express **19**(23), 23386–23399 (2011).
50. J. E. Sipe, C. Y. So, M. Fukui, and G. I. Stegeman, "Analysis of second-harmonic generation at metal surfaces," Phys. Rev. B **21**(10), 4389–4402 (1980).
51. R. W. Boyd, Nonlinear Optics (Academic Press, New York, 1992).
52. J. I. Dadap, J. Shan, K. B. Eisenthal, and T. F. Heinz, "Second-harmonic Rayleigh scattering from a sphere of centrosymmetric material," Phys. Rev. Lett. **83**(20), 4045–4048 (1999).
53. B. Metzger, T. Schumacher, M. Hentschel, M. Lippitz, and H. Giessen, "Third harmonic generation in complex plasmonic Fano structures," ACS Photon. **1**(6), 471–476 (2014).
54. A. E. Miroshnichenko, S. F. Mingaleev, S. Flach, and Y. S. Kivshar, "Nonlinear Fano resonance and bistable wave transmission," Phys. Rev. E Stat. Nonlin. Soft Matter Phys. **71**(3 3 Pt 2B), 036626 (2005).
55. H. Liu, G. X. Li, K. F. Li, S. M. Chen, S. N. Zhu, C. T. Chan, and K. W. Cheah, "Linear and nonlinear Fano resonance on two-dimensional magnetic metamaterials," Phys. Rev. B **84**(23), 235437 (2011).
56. S. Link, M. B. Mohamed, and M. A. El-Sayed, "Simulation of the optical absorption spectra of gold nanorods as a function of their aspect ratio and the effect of the medium dielectric constant," J. Phys. Chem. C **103**(16), 3073–3077 (1999).
57. H. Fischer and O. J. F. Martin, "Engineering the optical response of plasmonic nanoantennas," Opt. Express **16**(12), 9144–9154 (2008).
58. B. Hopkins, A. N. Poddubny, A. E. Miroshnichenko, and Y. S. Kivshar, "Revisiting the physics of Fano resonances for nanoparticle oligomers," Phys. Rev. A **88**(5), 053819 (2013).
59. V. K. Valev, "Characterization of nanostructured plasmonic surfaces with second harmonic generation," Langmuir **28**(44), 15454–15471 (2012).
60. J. Butet, S. Dutta-Gupta, and O. J. F. Martin, "Surface second-harmonic generation from coupled spherical plasmonic nanoparticles: Eigenmode analysis and symmetry properties," Phys. Rev. B **89**(24), 245449 (2014).
61. P. B. Johnson and R. W. Christy, "Optical constants of the noble metals," Phys. Rev. B **6**(12), 4370–4379 (1972).
62. F. X. Wang, F. J. Rodriguez, W. M. Albers, R. Ahorinta, J. E. Sipe, and M. Kauranen, "Surface and bulk contributions to the second-order nonlinear optical response of a gold film," Phys. Rev. B **80**(23), 233402 (2009).
63. G. Bachelier, J. Butet, I. Russier-Antoine, C. Jonin, E. Benichou, and P.-F. Brevet, "Origin of optical second-harmonic generation in spherical gold nanoparticles: Local surface and nonlocal bulk contributions," Phys. Rev. B **82**(23), 235403 (2010).
64. T. F. Heinz, *Second-Order Nonlinear Optical Effects at Surfaces and Interfaces, in Nonlinear Surface Electromagnetic Phenomena*, H.-E. Ponath and G. I. Stegeman (Elsevier, Amsterdam, 1991).
65. J. Butet, B. Gallinet, K. Thyagarajan, and O. J. F. Martin, "Second harmonic generation from periodic arrays of arbitrary shape plasmonic nanostructures: A surface integral approach," J. Opt. Soc. Am. B **30**(11), 2970–2979 (2013).

1. Introduction

Fano resonances have been observed in a huge variety of phenomena in various physical systems, ranging from the absorption profile in noble gases to the strong coupling between Mie and Bragg scattering in photonic crystals, as well as the autoionization of atoms [1–3]. Fano resonances are characterized by their asymmetric lineshape which arises from the interaction between a discrete state and a continuum of states, as described by the original formula derived by Ugo Fano [4]. The asymmetry of the response is explained by the spectral proximity of constructive and destructive interferences which results in very narrow features in the spectral response. More recently, Fano resonances have been observed in nanosystems, opening new possibilities for the control of light-matter interaction down to the nanoscsale [5]. Among all the possible nanostructures, plasmonic nanoparticles play an important role in nanophotonic, due to their ability to enhance the electromagnetic field intensity in tiny volumes. This enhancement and the corresponding electromagnetic field distribution can be very well controlled thanks to mode coupling in general and Fano resonances in particular [6, 7]. Fano resonances have been observed in plasmonic nanostructures with various geometries [8–19] and several theoretical methods have been developed with the purpose of understanding their properties [20–22]. The main difference with dielectric or atomic systems is that metallic nanoparticles are lossy [21, 23]. In this case, the original Fano's formula is not

#224277 - $15.00 USD Received 2 Oct 2014; revised 10 Nov 2014; accepted 10 Nov 2014; published 20 Nov 2014

able to reproduce the observed lineshapes with a high accuracy and a more general formula including losses has been recently derived [21, 23]. Determining the influence of the different parameters on the final lineshape is of prime importance for the design of efficient plasmonic sensors and metasurfaces [17, 18, 24]. To do so, several approaches such as coupled oscillator model or subgroup decomposition have been successfully developed [25, 26].

In the meantime, a particular attention has been paid to nonlinear optical processes in plasmonic systems [27]. Indeed, the strong near-field intensity close to plasmonic nanostructures results in nonlinear optical processes such as second harmonic generation (SHG) [28–31], multi-photon excited luminescence [32–34], third harmonic generation (THG) [35–38], four-wave mixing [39], and Kerr effect [40], to name a few. The influence of Fano resonances on the nonlinear response of plasmonic systems has been recently addressed, demonstrating both an enhancement and an unprecedented control of the nonlinear light generation at the nanoscale [41–45]. The enhancement of the nonlinear response is induced by the strong field localization associated with Fano resonances [41–43, 45]. Recently, advanced plasmonic sensors based on SHG were also proposed, exploiting either the possibility to observe multipolar surface plasmon resonances [46] or the asymmetry of the nonlinear emission [47]. As was done for the linear response, it is important for the design of efficient plasmonic sensors working in the nonlinear regime to understand and control the lineshape of Fano resonances in this particular regime [46, 47]. The simplest and most straightforward way is to generalize the methods previously developed for the linear response to its nonlinear counterpart [25, 26]. However, the potential of such an approach has not yet been addressed.

In this article, we investigate the outcomes of the coupled oscillator model and the subgroup decomposition for the comprehension of SHG from plasmonic systems supporting Fano resonances. The SHG from the considered plasmonic Fano metamolecules is computed using a surface integral equation method [48, 49] and the results are discussed in the light of these two approaches. First, a 4-nanorod nanostructure is considered and it is found that the coupled oscillator model allows us to decipher the multipolar nature of the second harmonic (SH) emission. In a second step, we show that both the main near-field and far-field properties of SHG from quadrumer and pentamer can be deduced from a suitable subgroup decomposition. These results provide a very appropriate framework for future experimental investigations on tailoring Fano resonance lineshapes in the nonlinear regime.

2. Results and discussion

2.1 Extended coupled oscillator model

The first plasmonic nanostructure discussed in this work is composed of four gold nanorods (see the inset in Fig. 1(a)) [26]. Two of the nanorods constitute a nanoantenna: their length is l = 70 nm and they are separated by a gap g = 25 nm. The nanoantenna is surrounded by two parallel nanorods with lengths L = 120 nm. The width and the thickness of all the nanorods are fixed to 40 nm and the lateral distance between the nanorods is 20 nm. The plasmonic nanostructure is excited by an incident planewave polarized along the long axis of the nanorods and propagating perpendicularly to the plane containing the nanostructure (see the inset in Fig. 1(a)). The backward scattered intensity is computed as a function of the incident wavelength. The result is shown in Fig. 1(a), revealing the asymmetric lineshape of a Fano resonance. The observation of a Fano resonance is explained as follows [26]. The modes supported by the dipolar nanoantenna (DA) and the dipolar nanorods (DN) interact resulting in new hybridized modes. Depending on the relative phase between the original modes supported by the DA and the DN, the hybridized mode is a superradiant mode (the original modes are in-phase) or a subradiant (dark) mode (the original modes are out-of-phase) [26]. The Fano resonance results from the interference between the two hybridized modes which spectrally overlap. As an example, the dip observed in the backward intensity spectrum is induced by destructive interferences between the hybridized modes [26].

#224277 - $15.00 USD Received 2 Oct 2014; revised 10 Nov 2014; accepted 10 Nov 2014; published 20 Nov 2014

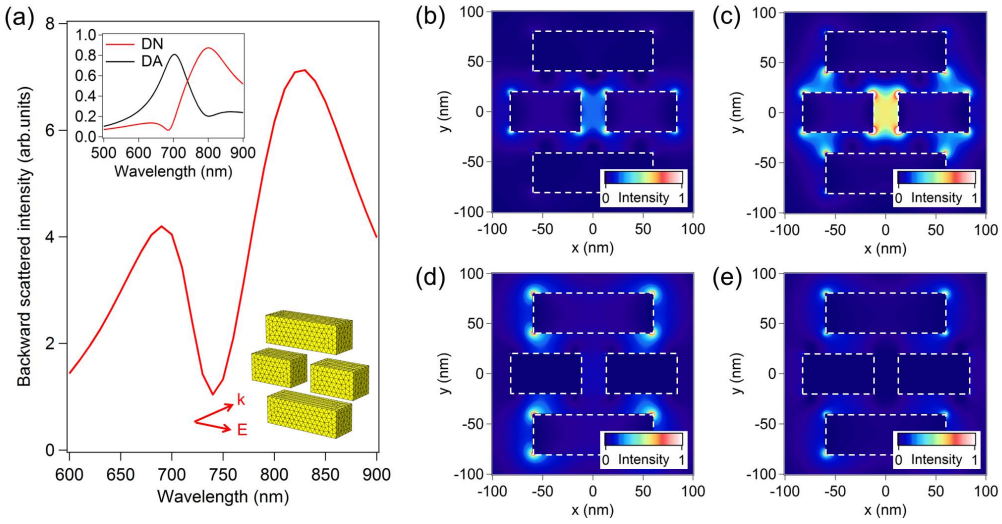

Fig. 1. Linear optical properties of the 4-nanorod gold nanostructure. (a) Backward scattered intensity as a function of the incident wavelength. First inset: amplitudes of the dipole moments associated with the nanoantenna (red curve) and with the long nanorods (black curve). See the main text for details of the model. Second inset: mesh used for the numerical computations. The length of top and bottom rods is L = 120 nm. The central nanoantenna is composed of two 70 nm nanorods separated by a gap g = 25 nm. The width and height of the nanorods are 40 nm. The nanostructure is driven by an incident planewave propagating perpendicularly to the structure and polarized along the nanorods long axis. Normalized near-field intensity close to the 4-nanorod structure for an incident wavelength (b) λ = 680 nm, (c) λ = 740 nm, (d) λ = 820 nm, and (e) λ = 900 nm.

In order to provide a clear insight into the mode coupling in this plasmonic metamolecule, an extended coupled oscillator (ECO) model has been developed and reported in [26]. This model is briefly discussed here but the reader is referred to this previous publication for further details [26]. In this model, the two original modes supported by the DA and the DN are associated to two oscillators coupled with a spring. Both the radiative and the non-radiative (intrinsic) losses are taken into account as required for the description of lossy plasmonic systems. The coupled oscillators are driven by an external force with a harmonic time dependence representing the excitation by the incident planewave. The equations of motions for the two oscillators can be written as [26]:

$$\begin{cases} \ddot{x}_1 + \gamma_1 \dot{x}_1 + \omega_1^2 x_1 + g x_2 = 0.5 \ddot{P}_{tot} + \alpha_1 E_{ext} \\ \ddot{x}_2 + \gamma_2 \dot{x}_2 + \omega_2^2 x_2 + g x_1 = 0.5 \ddot{P}_{tot} + \alpha_2 E_{ext} \end{cases} \quad (1)$$

where $\omega_{1,2}$ are the resonant frequencies, $\gamma_{1,2}$ are the damping constants, $x_{1,2}$ are the respective amplitude, $\alpha_{1,2}$ are the polarizabilities, E_{ext} is the incident electric field, g is the constant of the coupling spring, and P_{tot} is the total dipole moment. Fitting the scattering spectrum with this extended coupled oscillator (ECO) model permits to determine the excitation strengths of the original modes which are buried in the total response. The amplitudes of the modes supported by the DA (black curve) and the DN (red curve) are shown in the inset in Fig. 1(a). In order to confirm the prediction of the ECO model, the intensity close to the 4-nanorod structure was computed for several incident wavelengths ranging from λ = 680 nm to λ = 900 nm and corresponding to different excitation strengths of the original plasmonic modes. Interestingly, specific near-field intensity distributions are observed for specific incident wavelengths. In particular, the near-field intensity is concentrated close to DA for an incident wavelength λ = 680 nm and close to the DN for the incident wavelength λ = 820 nm in agreement with the ECO model, demonstrating that the original modes can be selectively excited with the proper

#224277 - $15.00 USD Received 2 Oct 2014; revised 10 Nov 2014; accepted 10 Nov 2014; published 20 Nov 2014

excitation wavelength despite the mode hybridization [26]. For intermediate (λ = 740 nm) or longer (λ = 900 nm) wavelengths, the distributions of the intensity close to the 4-nanorod structure show that the two modes supported by both the DA and the DN are effectively excited in these cases. The fundamental intensity distribution over the nanorods surface is an important parameter that dramatically influences their nonlinear response, as recently discussed in the case of the SHG from gold nanodolmens [44]. Indeed, the strength of the SH source standing at a given point of the metallic surface depends on the local fundamental intensity evaluated at this point (just below the interface – in gold) [50]. In the following, the SH response of the 4-nanorod nanostructure is discussed in details and the outcome of the ECO model for the understanding of the nonlinear response is addressed.

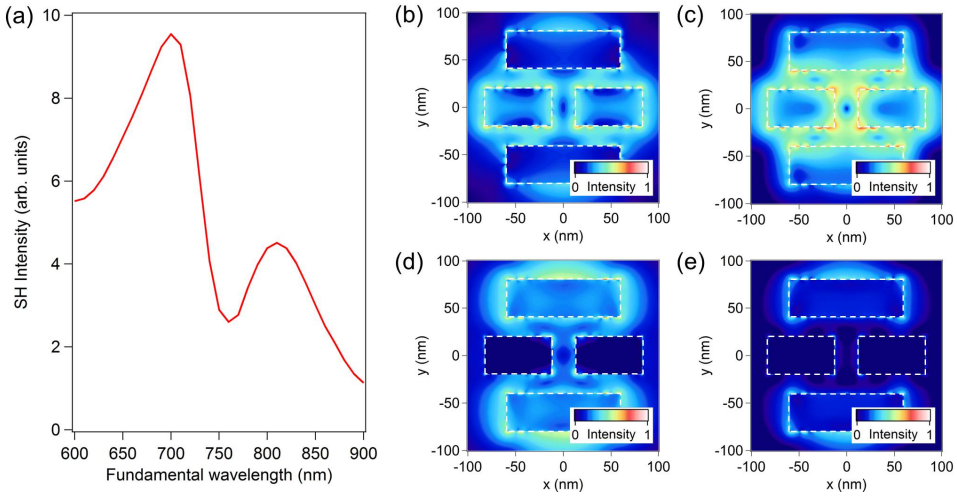

Fig. 2. (a) SH intensity for the 4-nanorod structure as a function of the fundamental wavelength. The SH intensity has been integrated over a sphere with a 50 μm radius. The excitation conditions are identical to that of Fig. 1. Normalized near-field SH intensity close to 4-nanorod structure for an incident wavelength (b) λ = 680 nm, (c) λ = 740 nm, (d) λ = 820 nm, and (e) λ = 900 nm.

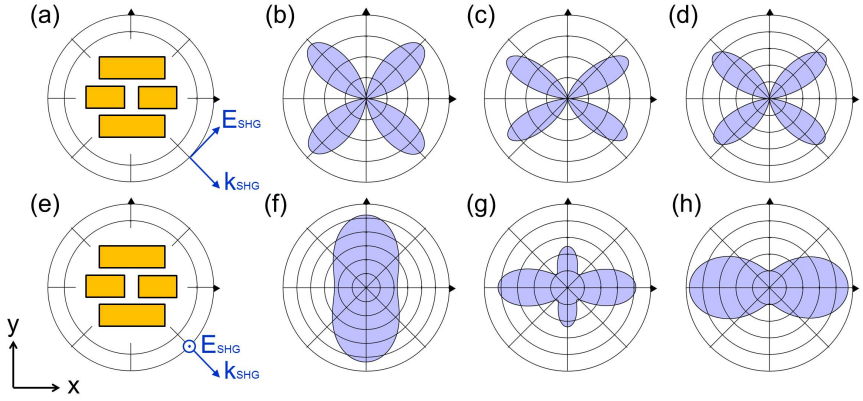

Fig. 3. Normalized SH intensity scattered in the vertical (O, x, y) plane as a function of the scattering angle considering the SH scattered wave polarized (a)-(d) into and (b)-(h) perpendicularly to the vertical plane. The fundamental wavelength is (b), (f) 680 nm, (c), (g) 740 nm, and (d), (h) 840 nm.

The nonlinear optical response of the 4-nanorod structure has been computed using a surface integral equation method adapted and developed for surface SHG [49]. Indeed, SHG

#224277 - $15.00 USD Received 2 Oct 2014; revised 10 Nov 2014; accepted 10 Nov 2014; published 20 Nov 2014

is forbidden in the bulk of centrosymmetric media within the electric dipole approximation [50]. However, the centrosymmetry is locally broken at the interface between two centrosymmetric media resulting in the generation of a SH wave [51]. Figure 2(a) shows the SH intensity from the 4-nanorod structure as a function of the fundamental wavelength. The SH intensity has been integrated over a sphere with radius r = 50 μm. As was the case for the linear response, the SH spectrum is asymmetric, composed of two maxima separated by a dip, and appears to be also a Fano resonance. However, the exact Fano lineshape differs from the one observed in the linear regime. This is due to several reasons. First, the wavelength dependence of the SH intensity is different from that of linear scattering. The studied nanostructure is centrosymmetric and the SH response is induced by retardation effect, i.e. the electromagnetic field variation over the considered nanostructure [52]. As a consequence, the scattered SH intensity tends to increase as the fundamental wavelength decreases. Second, the SH intensity increases due to the excitation of the localized surface plasmon modes [52]. This enhancement is directly related to the amplification of the local fundamental intensity at the nanostructure surface induced by plasmonic resonances in the metal. In order to understand the role played by the enhancement of fundamental near-field intensity in the increase of the nonlinear response, the near-field SH intensity close to the 4-nanorod structure was computed for several incident wavelengths ranging from $\lambda = 680$ nm to $\lambda = 900$ nm. The near-field distribution of the SH intensity is strongly correlated to that of the fundamental intensity, predicting that the enhancement of SHG is closely related to the excitation of the mode supported by the DA and the DN. Since the near-field distribution of the fundamental intensity is predicted by the ECO model, at least which nanorods are excited (the DA and/or the DN), one can expect to deduce some properties of the SHG from this model. This approach has already been used to describe the THG from gold nanoantennas [37] and has been recently extended to the THG from plasmonic systems supporting Fano resonances [53]. In this model, one third harmonic mode is associated with each fundamental mode [53]. This one-to-one correspondence does not stand in the case of SHG from plasmonic systems. Indeed, SHG from plasmonic nanostructures with centrosymmetric shapes is forbidden in the electric dipole approximation. A logical outcome is that high order modes, i.e. quadrupolar modes, must be included in the SH response [28, 29]. For example, the electric dipole mode driven at the fundamental wavelength can couple to itself to generate a quadrupolar SH emission [52]. The other possibility is the coupling of the electric dipole mode with a high order mode at the fundamental wavelength. In this latter case, the nature of the SH emission can correspond to that of an electric dipole. A straightforward way for addressing the multipolar nature of the SH emission and determining the relative weight of the different multipoles is to consider the emission pattern in the scattering plane perpendicular to the incident planewave [29]. Interestingly, analyzing the polarization of the SH emission in this plane enables the separation of the modes with even and odd parity [29]. The SH intensity scattered in the vertical (O, x, y) plane is shown in Fig. 3 as a function of the scattering angle for three different fundamental wavelengths $\lambda = 680$ nm, $\lambda = 740$ nm, and $\lambda = 840$ nm. For the SH wave polarized into the vertical plane, a four-lobe pattern, which is characteristic of a quadrupolar emission, is always observed. On the contrary, the emission pattern obtained for the SH wave polarized perpendicularly to the vertical plane evolves when the fundamental wavelength changes.

#224277 - $15.00 USD Received 2 Oct 2014; revised 10 Nov 2014; accepted 10 Nov 2014; published 20 Nov 2014

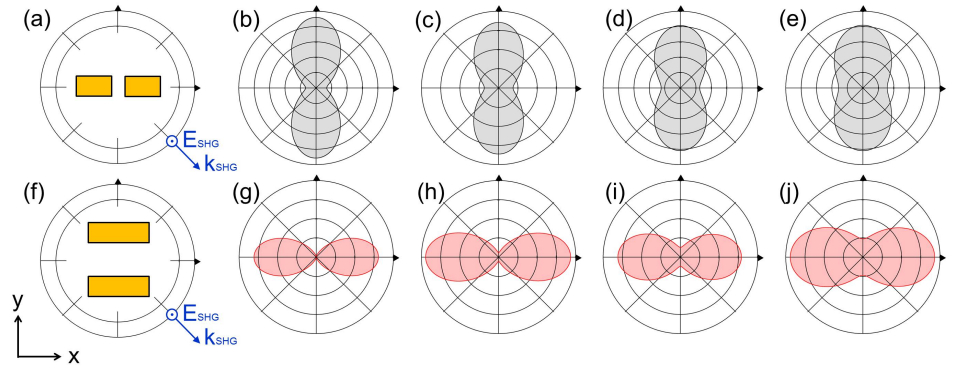

Fig. 4. Normalized SH intensity scattered in the vertical (O, x, y) plane as a function of the scattering angle considering the SH scattered wave polarized perpendicularly to the vertical plane for (a)-(e) the nanoantenna and (f)-(j) the two parallel nanorods. The fundamental wavelength is (b),(g) 680 nm, (c),(h) 740 nm, (d),(i) 820 nm, and (e),(j) 900 nm.

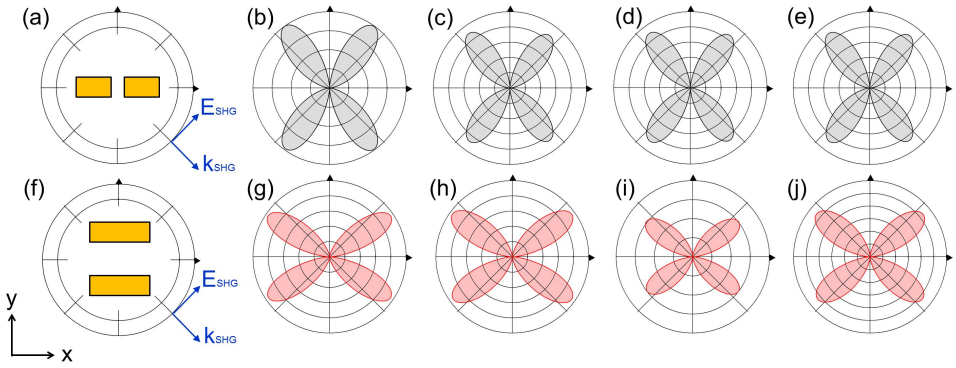

Fig. 5. Normalized SH intensity scattered in the vertical (O, x, y) plane as a function of the scattering angle considering the SH scattered wave polarized into the vertical plane for (a)-(e) the nanoantenna and (f)-(j) the two parallel nanorods. The fundamental wavelength is (b),(g) 680 nm, (c),(h) 740 nm, (d),(i) 820 nm, and (e),(j) 900 nm.

In order to understand this evolution, the SHG from the DA and the DN, the building blocks of the 4-nanorod nanostructure, has been evaluated in the same condition (see Figs. 4 and 5). The results indicate that the SHG from the DA is preferentially scattered in the downward and upward directions (along the y-axis), while the SHG from the DN is preferentially scattered in the lateral directions (along the x-axis). This information, combined with the one provided by the ECO model, provides a full understanding on how the emission pattern evolves with the incident wavelength. For the shortest studied wavelength (λ = 680 nm), the SH wave is preferentially scattered in the downward and upward directions, as observed for the SHG from the DA, while the SH wave is preferentially scattered in the lateral direction for an incident wavelength λ = 840 nm, as observed for the SHG from the DN. This observation is in agreement with the ECO model which predicts that the DA, respectively the DN, are resonantly excited at λ = 680 nm, respectively λ = 840 nm. For the intermediate wavelength (λ = 740 nm), the SH emission pattern exhibits maxima along both the x- and the y-axis. In this spectral region, the ECO model indicates that the electric dipole modes supported by the DN and the DA have approximately the same amplitude (see the inset in Fig. 1) and the total SH field results from the interference between the nonlinear emissions of the DN and the DA. In first approximation, the final emission pattern is a function of the relative phase and amplitude of the original modes supported by the DA and DN (given by the ECO model) convolved with the spectral dependence of the SHG from the isolated DA and DN

#224277 - $15.00 USD Received 2 Oct 2014; revised 10 Nov 2014; accepted 10 Nov 2014; published 20 Nov 2014

(accessible with full wave computation - see Figs. 4 and 5). Even though the ECO model does not lead to the complete SH wave due to its complex multipole decomposition, it is found that this model provides very useful information for the understanding of Fano resonances in the SHG from plasmonic systems.

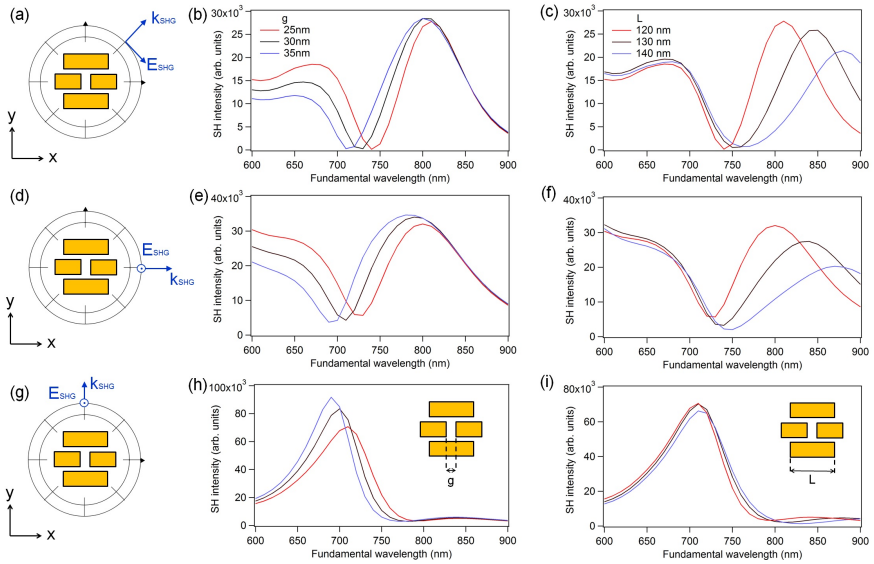

Fig. 6. (a-c) SH intensity scattered in the vertical (O, x, y) plane with a scattering angle of 45° and polarized into the vertical plane. This configuration is closely related to the intensity of the quadrupolar emission (see Fig. 3). (d-f) SH intensity scattered along the x-axis and polarized perpendicularly to the vertical plane (along the z-axis). (g-i) SH intensity scattered along the y-axis and polarized perpendicularly to the vertical plane (along the z-axis). (b),(e),(h) SH intensity as a function of the fundamental wavelength for different distances between the nanoantenna arms: g = 25 nm (red curves), g = 30 nm (black curves), and g = 35 nm (blue curves). (c),(f),(i) SH intensity as a function of the fundamental wavelength for different long rod lengths: L = 120 nm (red curves), L = 130 nm (black curves), and L = 140 nm (blue curves).

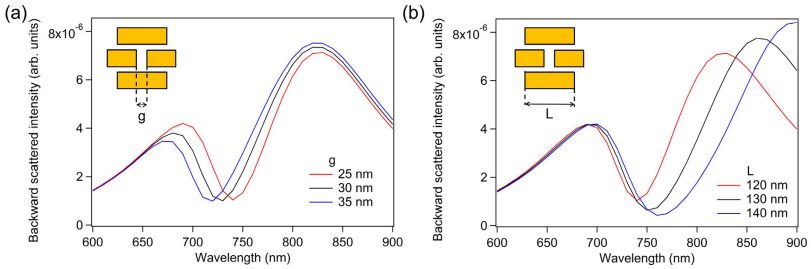

Fig. 7. Backward scattered intensity as a function of the incident wavelength for (a) various gaps g and (b) lengths L.

As mentioned in the previous paragraph, the nonlinear spectral responses of the DA and the DN are important parameters for determining the properties of the nonlinear Fano resonance arising in the 4-nanorod nanostructure. Note that the terminology “nonlinear Fano resonance” refers here to a Fano resonance involved in a nonlinear process [54, 55]. The spectral responses of the DA and the DN can be tuned by modifying some of their geometric parameters. Increasing the length L of the DN increases their aspect ratio, resulting in a redshift of the corresponding resonance [56]; while increasing the distance g between the two arms of the nanoantenna reduces the mode coupling, resulting in a blueshift of the resonance

#224277 - $15.00 USD Received 2 Oct 2014; revised 10 Nov 2014; accepted 10 Nov 2014; published 20 Nov 2014

supported by the DA [57]. In order to address the influence of the building block properties on the nonlinear Fano resonance and the multipole expansion of the SH response, computations have been performed for various values of the DN length L and the distance g between the arms of the DA, for incident wavelengths ranging from 600 nm to 900 nm (Fig. 6). The influence on the linear back scattered intensity is shown in Fig. 7 for direct comparison. Several configurations for the evaluation of the SH far-field intensity have been considered in order to study the influence of the different multipoles. In the first configuration, the SH intensity is evaluated in the vertical (O, x, y) plane, with a scattering angle of 45°, for the SH wave polarized into the vertical plane. This configuration provides the spectral dependence of the quadrupolar SH emission. The result is shown in Fig. 6(b) for various gaps g (the DN length L is kept constant) and in Fig. 6(c) for various DN lengths L (the gap g is kept constant). As previously observed for the case of the total SH intensity, the different spectra reveal the asymmetric lineshapes of Fano resonances. In this configuration, both the DN and the DA radiate at the SH wavelength as quadrupole (see Fig. 5) and these emissions interfere in the far-field when DN and the DA are assembled into a 4-nanorod nanostructure. The phase and the amplitude of the quadrupolar emissions depend on that of the original modes supported by the DA and DN (given by the ECO model) convolved with the spectral dependence of the SHG from the isolated DA and DN (in first approximation). When one of these original modes is shifted due to a geometric modification of the supporting nanostructure, the Fano lineshape evolves and both the width and the spectral position of the Fano dip are tuned, demonstrating that the nonlinear emission can be controlled by the Fano resonance. It is worth mentioning that the spectral shifts of the peaks have the same amplitude in both the linear and the nonlinear regime (see Figs. 6 and 7). This observation confirms the potential of the ECO model for predicting the influence of Fano resonances on the nonlinear response of coupled plasmonic nanostructures. Considering the SH wave polarized perpendicularly to the vertical plane for example (see panels (d)-(i) in Fig. 6), the same trend is observed for the SH wave scattered in the lateral direction (along the x-axis – panels (d)-(f)) while the SH wave scattered along the y-axis (panels (g)-(i)) is modified only when the DA is tuned. Indeed, in this case, the SH intensity originates mainly from the DA and the influence of the DN, i. e. the interference contrast, is very weak demonstrating that the nonlinear emission from specific gold nanorods can be selectively observed.

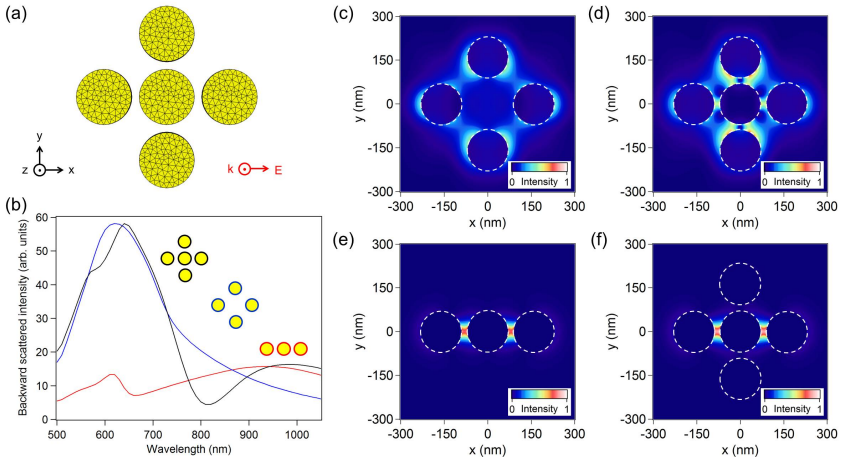

Fig. 8. Linear optical properties of the gold pentamer and of its two subgroups. (a) Mesh used for the numerical computations. The disk diameter is 140 nm and the height is 60 nm. The interparticle distance is 20 nm. The gold pentamer and the subgroup structures are driven by an incident planewave propagating perpendicularly to the structure and polarized along the x-axis. (b) Backward scattered intensity as a function of the incident wavelength for the complete pentamer (black curve), the subgroup I (blue curve), and the subgroup II (red curve). Normalized near-field intensity close to (c) the subgroup I, (d)-(f) the complete pentamer, and (e) the subgroup II. The incident wavelength is (c)-(d) $\lambda = 620$ nm and (e)-(f) $\lambda = 930$ nm.

#224277 - $15.00 USD Received 2 Oct 2014; revised 10 Nov 2014; accepted 10 Nov 2014; published 20 Nov 2014

2.2 Subgroup decomposition

The coupling oscillator model is not the only approach introduced for understanding and predicting the spectral lineshape of Fano resonances in plasmonic systems. The subgroup decomposition has proven itself to be a very efficient and simple approach for doing so, despite its empirical nature [25]. Note that a more formal eigenmode decomposition has been recently proposed [58]. The basic idea of the subgroup decomposition is to intuitively decompose the whole spectrum into two separate contributions from subgroups of nanoparticles [25]. The two subgroups are identified as those supporting the resonances corresponding to the two dominant peaks of the whole spectrum using a similar approach to that detailed in [25]. As an example, let us consider a centrosymmetric pentamer composed of 5 gold nanodisks (Fig. 8). The disks diameter is 140 nm and their height is 60 nm. The interparticle distance is 20 nm. It was shown that the linear optical response of this pentamer can be decomposed into that of a quadrumer, for which the central nanodisk is removed (subgroup I), and that of a linear trimer along the incident electric field (subgroup II) [25]. The backward scattered intensity is shown in Fig. 8(b) as a function of the incident wavelength for the complete pentamer (black curve), the subgroup I (blue curve), and the subgroup II (red curve). Note that the dip in the scattering close to λ = 800 nm is due to destructive interference between the fields scattered by the two subgroups [25]. In this spectral region, the modes supported by the two subgroups are out of phase, resulting in a decrease of the scattered intensity. In order to further confirm the potential of the subgroup decomposition, it is also possible to consider the intensity distribution in the near-field region. Comparing the near-field intensity close to the whole pentamer and to the subgroups I and II for incident wavelengths which are closed to their resonance wavelengths (λ = 620 nm for subgroup I and λ = 930 nm for subgroup II) also reveals similar trends [25]. As an example, the intensity enhancement in the gap between the nanoparticles is clearly observed for both the complete pentamer and the subgroup II (λ = 930 nm). This observation is important for extending the subgroup decomposition to the nonlinear regime. Indeed, SHG is directly related to the fundamental near-field intensity distribution through the surface nonlinear polarization.

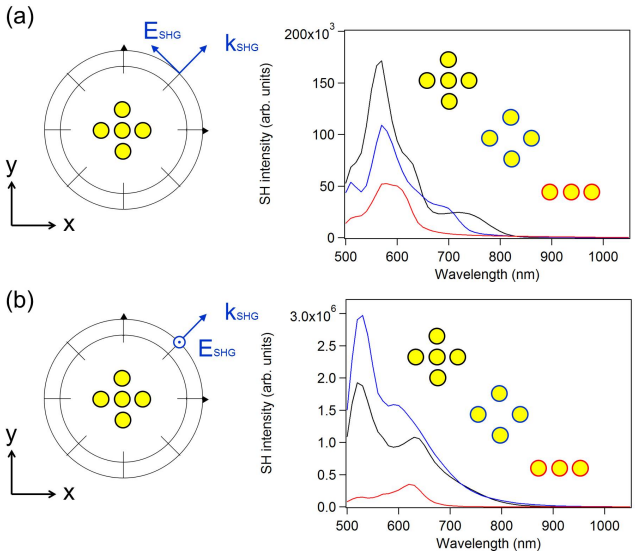

Fig. 9. SHG from the gold pentamer and from its two subgroups. (a) SH intensity scattered in the vertical (O, x, y) plane with a scattering angle of 45° and polarized into the vertical plane: complete pentamer (black curve), the subgroup I (blue curve), and the subgroup II (red curve). (b) SH intensity scattered in the vertical (O, x, y) plane with a scattering angle of 45° and polarized perpendicularly to the vertical plane (along the z-axis): complete pentamer (black curve), the subgroup I (blue curve), and the subgroup II (red curve).

#224277 - $15.00 USD Received 2 Oct 2014; revised 10 Nov 2014; accepted 10 Nov 2014; published 20 Nov 2014

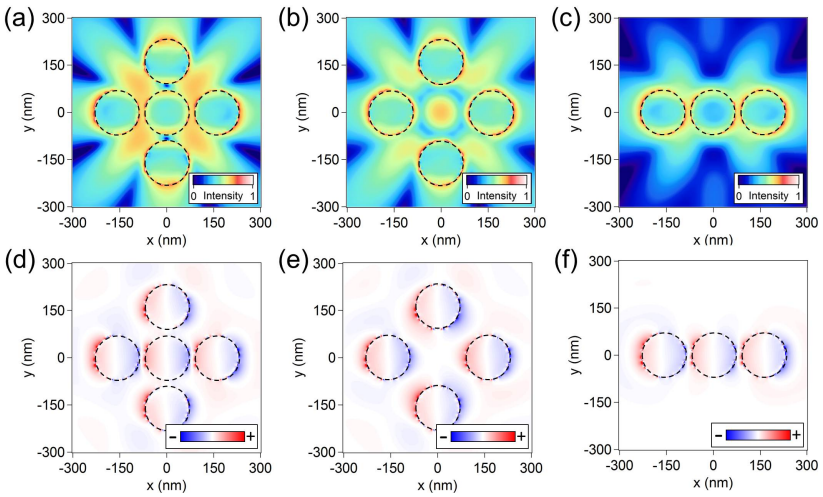

Fig. 10. Normalized near-field SH intensity close to (a) the complete pentamer, (b) subgroup I, and (c) the subgroup II. The incident wavelength is λ = 520 nm. The real part of the x-component of the second harmonic electric field Re(Ex) close to (d) the complete pentamer, (e) subgroup I, and (f) the subgroup II.

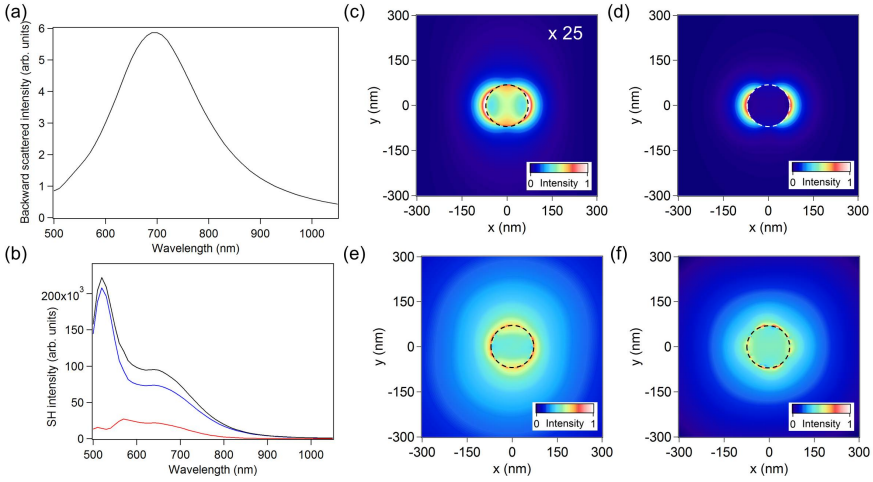

Fig. 11. (a) Backward scattered intensity as a function of the incident wavelength for a single nanodot. The disk diameter is 140 nm and the height is 60 nm. (b) SH intensity scattered in the vertical (O, x, y) plane with a scattering angle of 45° and polarized into the vertical plane (red curve), perpendicularly to the vertical plane (blue curve), and the total intensity (black curve). Normalized near-field intensity close to the nanodot: The incident wavelength is (c) λ = 520 nm and (d) λ = 700 nm. Normalized near-field SH intensity close to the nanodot: The incident wavelength is (e) λ = 520 nm and (f) λ = 700 nm.

In order to investigate the potential of the proposed subgroup decomposition for the understanding of the SH response, the SHG from the whole pentamer, the subgroup I and the subgroup II, has been computed using the same surface integral equation method (Figs. 9 and 10). The SH intensity scattered in the vertical (O, x, y) plane with a scattering angle of 45° is shown for the SH wave polarized into the vertical plane (Fig. 9(a)) and perpendicularly to the vertical plane (Fig. 9(b)). As in the linear regime, the main features of the SHG from the whole pentamer are already observed in the SH response of the two subgroups; for example the peak at λ = 570 nm, the shoulder at λ = 750 nm (slightly redshifted in comparison with the SHG from the subgroup I) and the near-field distribution. For comparison, the SHG from a

#224277 - $15.00 USD Received 2 Oct 2014; revised 10 Nov 2014; accepted 10 Nov 2014; published 20 Nov 2014

single nanodot is shown in Fig. 11. Note that the fundamental electric field is evaluated inside the metal, explaining the strong SHG at 520 nm despite relatively weak electric field outside the gold nanodot [50]. As previously observed for the ECO model, the subgroup decomposition provides useful and important information for predicting the SH response of coupled plasmonic systems. Contrary to the 4-nanorod nanostructures, some of the gold nanodots are included in the two subgroups in the present decomposition. It is interesting to note that the overall emission can be retrieved from the subgroup decomposition despite the nonlinear dependence of SHG on the fundamental near-field intensity.

SHG is also sensitive to the symmetry of the plasmonic nanostructure geometric organization [59]. In order to investigate the potential of the subgroup decomposition for the understanding of SHG from gold nanodots with a non-centrosymmetric spatial organization, both the linear and the SH responses of a quadrumer were computed and the results are shown in Figs. 12, 13 and 14. The quadrumer is decomposed into two subgroups with triangular geometries [25]: the subgroup I is composed of the three external nanodots (the central nanodot is removed) and the subgroup II corresponds to a smaller triangle for which the bottom nanodot has been removed. Note that the complete quadrumer and the two subgroups exhibit a non-centrosymmetric spatial organization. As observed in the case of the centrosymmetric pentamer, the main features of the SHG from the whole quadrumer are already observed in the SH response of the two subgroups. However, some specific features, such as the strong near-field interaction between the central and the bottom nanoparticles, are not reproduced by the subgroup decomposition. This lack is already observed in the linear regime and appears to be a limitation of the subgroup decomposition for specific cluster geometries. As an example, this discrepancy could explain that specific features of the SH field are not perfectly reproduced (such as the small peak around 580 nm in Fig. 13(a)). It is interesting to note that the SH intensity is not dramatically increased in comparison with the pentamer discussed previously, despite the lack of centrosymmetry (compare Figs. 9 and 13). The breaking of centrosymmetry is expected to increase the SH intensity only in the backward and forward directions but not necessary in other scattering directions, explaining the similar amplitude of the computed SH signal. Even though the spatial organizations of the gold nanodots in the quadrumer and the two corresponding subgroups are non-centrosymmetric, the (O, x, z) plane is a symmetry plane, meaning that the nonlinear sources tend to be out-of-phase (see Fig. 14(d)-(f)) [58]. These results demonstrate the generality of the subgroup decomposition in the nonlinear regime, even for a non-centrosymmetric spatial organization.

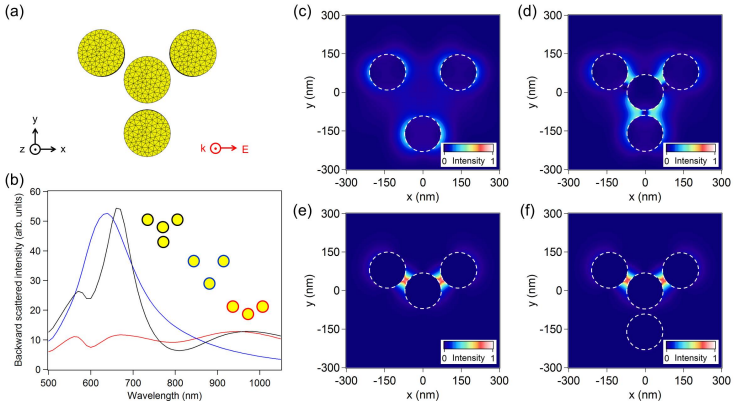

Fig. 12. Linear optical properties of the gold quadrumer and of its two subgroups. (a) Mesh used for the numerical computations. The disk diameter is 140 nm and the height is 60 nm. The interparticle distance is 20 nm. The gold quadrumer and the subgroups structures are driven by an incident planewave propagating perpendicularly to the structure and polarized along the x-axis. (b) Backward scattered intensity as a function of the incident wavelength for the complete quadrumer (black curve), the subgroup I (blue curve), and the subgroup II (red curve). Normalized near-field intensity close to (c) the subgroup I, (d)-(f) the complete quadrumer, and (e) the subgroup II. The incident wavelength is (c)-(d) $\lambda = 660$ nm and (e)-(f) $\lambda = 1000$ nm.

#224277 - $15.00 USD Received 2 Oct 2014; revised 10 Nov 2014; accepted 10 Nov 2014; published 20 Nov 2014

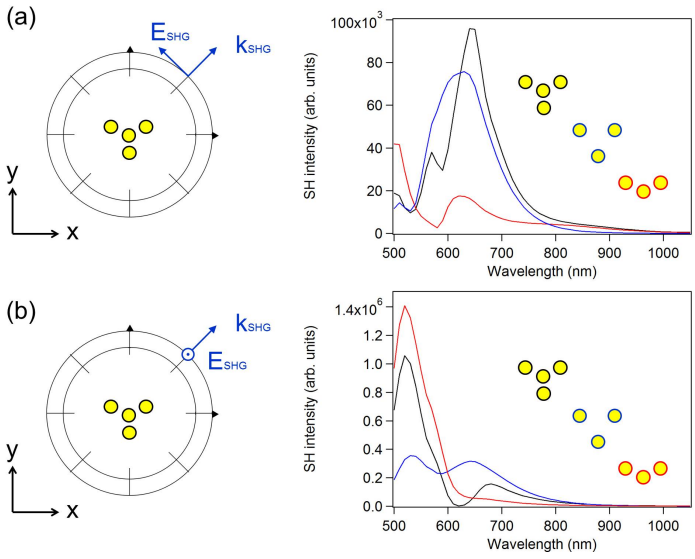

Fig. 13. SHG from the gold quadrumer and from its two subgroups. (a) SH intensity scattered in the vertical (O, x, y) plane with a scattering angle of 45° and polarized into the vertical plane: complete quadrumer (black curve), the subgroup I (blue curve), and the subgroup II (red curve). (b) SH intensity scattered in the vertical (O, x, y) plane with a scattering angle of 45° and polarized perpendicularly to the vertical plane (along the z-axis): complete quadrumer (black curve), the subgroup I (blue curve), and the subgroup II (red curve).

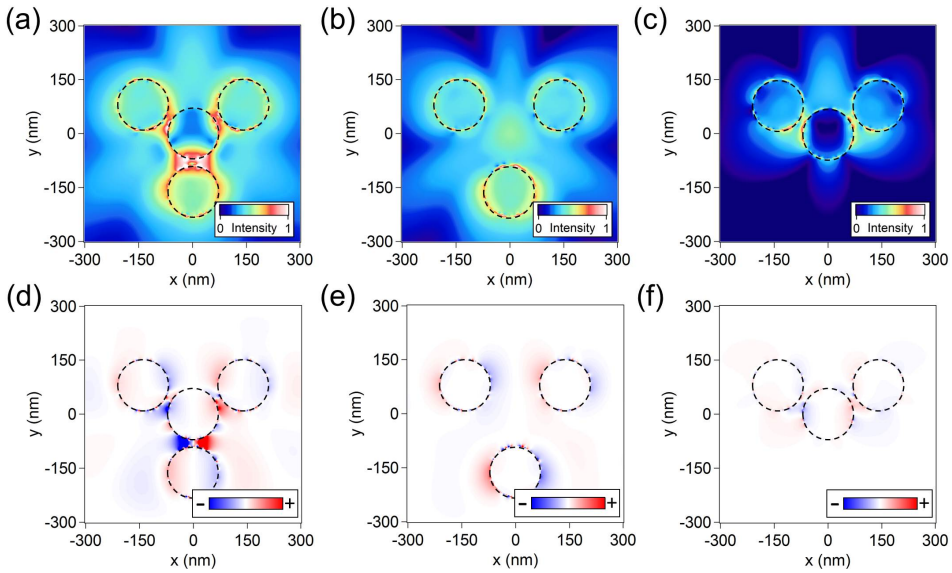

Fig. 14. Normalized near-field SH intensity close to (a) the complete quadrumer, (b) subgroup I, and (c) the subgroup II. The incident wavelength is λ = 660 nm. The real part of the x-component of the second harmonic electric field Re(Ex) close to (d) the complete quadrumer, (e) subgroup I, and (f) the subgroup II.

3. Conclusions

In summary, the outcomes of the ECO model and the subgroup decomposition for the comprehension of SHG from plasmonic systems supporting Fano resonances have been

#224277 - $15.00 USD Received 2 Oct 2014; revised 10 Nov 2014; accepted 10 Nov 2014; published 20 Nov 2014

investigated in details using a surface integral equation method. Different Fano metamolecules have been considered, demonstrating that these two models provide very useful information for understanding Fano resonances in the nonlinear regime. These results provide a versatile framework for tailoring Fano resonance lineshapes in the nonlinear regime, which is very important for the design of efficient plasmonic sensors based on nonlinear optics, especially second-order nonlinear optical processes [44, 47]. Indeed, it was demonstrated that SHG is a powerful tool for the observation of higher multipolar modes with narrow resonances which are interesting for sensing applications [46]. This work provides a comprehensive framework for the combination of the most efficient plasmonic sensors supporting Fano resonances and nonlinear optics in order to push forward the sensitivity of plasmonic sensors [46, 47]. Furthermore, the results presented in this work can be extended to other nonlinear spectroscopy techniques, like THG, thereby offering new possibilities for the design of nonlinear Fano resonances. In the future, it will be interesting to develop a complete description based on the ECO model and/or eigenmode analysis for both the linear and nonlinear responses in order to fully understand the influence of Fano resonances on nonlinear optical processes [60].

4. Methods

The linear optical responses have been calculated using a surface integral formulation. All the nanostructures are considered in water (n = 1.33) and the dielectric constants for gold are taken from experimental data at both the fundamental and second harmonic wavelengths [61]. For the SHG computations, the linear surface currents, which are expanded on Rao-Wilton-Glisson (RWG) basis functions, are used for the evaluation of the fundamental electric fields just below the gold surfaces and then used for the calculation of the surface SH polarization. For the sake of simplicity, only the component of the surface tensor, where n denotes the component normal to the surface, is considered. Recent experimental results shows that this term dominates the surface response of metallic nanoparticles [62, 63].The SH surface currents are obtained solving the SIE formulation taking into account the nonlinear polarization and enforcing the boundary conditions at the nanostructure surfaces [64]. As the linear surface currents, the SH surface currents are also expanded on RWG basis functions. The expanding coefficients are found applying the method of moments with Galerkin's testing [49, 65]. A Poggio-Miller-Chang-Harrington-Wu formulation is used to ensure accurate solutions even at resonant conditions [49, 65]. The SH electric field is then deduced from the SH surface currents using a two-term subtraction method for the evaluation of the Green's functions [49, 65].

Acknowledgments

It is a pleasure to acknowledge A. Lovera for providing us with the results of the ECO model. Funding from the Swiss National Science Foundation (projects 200020_153662 and 406440_131280) is gratefully acknowledged.